LANGMUIR

pubs.acs.org/Langmuir Article

Electroactive Nanogel Formation by Reactive Layer-by-Layer Assembly of Polyester and Branched Polyethylenimine via Aza-Michael Addition

Oyku Yildirimkaraman, Sezer Özenler, Ufuk Saim Gunay, Hakan Durmaz, and Ümit Hakan Yıldız*

Cite This: *Langmuir* 2021, 37, 10902−10913 Read Online

ACCESS | Metrics & More | Article Recommendations | Supporting Information

ABSTRACT: We here demonstrate the utilization of reactive layer-by-layer (rLBL) assembly to form a nanogel coating made of branched polyethylenimine (BPEI) and alkyne containing polyester (PE) on a gold surface. The rLBL is generated by the rapid aza-Michael addition reaction of the alkyne group of PE and the $-NH_2$ groups of BPEI by yielding a homogeneous gel coating on the gold substrate. The thickness profile of the nanogel revealed that a 400 nm thick coating is formed by six multilayers of rLBL, and it exhibits 50 nm roughness over 8 μm distance. The LBL characteristics were determined via depth profiling analysis by X-ray photoelectron spectroscopy, and it has been shown that a 70−100 nm periodic increase in gel thickness is a consequence of consecutive cycles of rLBL. A detailed XPS analysis was performed to determine the yield of the rLBL reaction: the average yield was deduced as 86.4% by the ratio of the binding energies at 286.26 eV, (C═CN−C bond) and 283.33 eV, (C≡C triple bond). The electrochemical characterization of the nanogels ascertains that up to the six-multilayered rLBL of BPEI-PE is electroactive, and the nanogel permeability had led to drive mass and charge transfer effectively. These results promise that nanogel formation by rLBL films may be a straightforward modification of electrodes approach, and it exhibits potential for the application of soft biointerfaces.

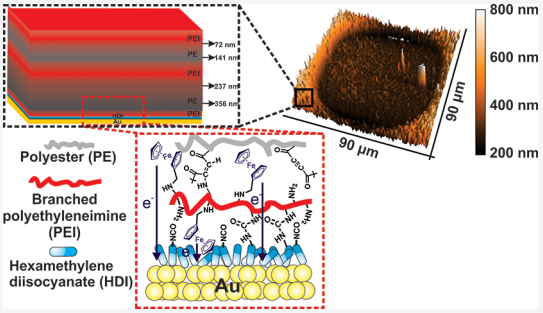

INTRODUCTION

Reactive layer-by-layer assembly (rLBL) emerges as a multilayered grafting methodology providing robust, erosion-resistant, post-functionalizable polymer coating on solid substrates.[1,2] Unlike noncovalent layer-by-layer assembly using electrostatic interactions, hydrogen bonding, and host−guest interactions, rLBL utilizes mutual reactions between interfacial polymer layers and propagates by rapid cross-linking of available functional groups. Earlier studies have exploited condensation reactions between nucleophiles and carbonyl groups for rLBL. Bergbreiter et al. have exemplified the use of poly(maleic anhydride)-c-poly(methyl vinyl ether) copolymer as an electrophile to provide the nucleophilic attack of amine- or hydroxyl-terminated generation five (G5) poly(amidoamine) or G5 poly(iminopropane-1,3-diyl) dendrimers.[3−5] Later, Lynn et al. showed nucleophilic addition of the amines of polyethylenimine (PEI) to the carbonyl group of poly(2-vinyl-4,4-dimethlyazalactone) via a stepwise LBL click.[6] Cu (I) catalyzed azide−alkyne [3 + 2] cycloadditions forming 1,2,3-triazoles were first used by the Caruso group for covalent LBL on quartz substrates.[7] Hawker et al. also showed the use of the [3 + 2] cycloadditions for LBL assembly on silicon wafers.[8] rLBL thin films have been extensively exploited for intriguing applications; for example, ultrahigh stiff free-standing films with a tensile strength of 15.6 GPa, approaching that of hard ceramics, have been shown by Kotov et al.[9] Epoxy/PEI made of rLBL was also suggested by Decher et al. for the improvement of abrasion resistance. The rLBL protected films had exhibited only 2% loss after 25 abrasion cycles.[10] rLBL strategy has been also exploited to improve antifouling properties of a surface and free-standing films; for instance, post-modification of PEI and poly(acrylic acid) (PAA) multilayers with polyethylene glycol (PEG) had led to preserve surface wettability and thereby provide good protection against biofouling over five months.[11] Moreover, rLBL methods were also adopted for increasing the biocompatibility of substrates.[12−14] Electrodes modified by rLBL multilayers have shown several advantages such as high anticorrosiveness, low loss in capacitance after charge−discharge cycles, and stable sensing performance after long storage periods.[15−22] A rationally designed rLBL modified electrode provides critical advantages for biosensor technologies such as increasing the biocompatibility and abrasion

Received: April 19, 2021
Revised: July 18, 2021
Published: September 3, 2021

https://doi.org/10.1021/acs.langmuir.1c01070
Langmuir 2021, 37, 10902−10913

protection, controlled mass and charge diffusion, controlled electron transfer, and higher immobilization efficiency.[23−25] Qu et al. conducted a glucose sensing study which revealed that a rLBL-based nanogel modified with a large amount of ferrocene has potential for sensing. The proposed nanogel-based glucose biosensor with high sensitivity, wide linear range, short response time, and good stability has been achieved in favor of improved enzyme loading and efficient electron transfer.[26] However, in the study, the nanogel does not covalently bond to the electrode surface. In another study Freeman et al. showed the use of a nanomaterial supported electrode containing hexanediol protected gold nanoparticles (NP) in a xerogel matrix for an amperometric glucose biosensor. The NP-doped xerogels provided a doubling of the linear range, improvement of sensitivity of an order, and four times faster response time accompanied by long-term stability.[27] Zhai, D. et al. obtained glucose sensor with Pt nanoparticle (NP)/polyaniline (PAni) heterostructured hydrogel. The generated three-dimensional porous structured sensor synergizes the advantages of both conductive hydrogel and nanoparticle catalyst. The high sensitivity up to 96.1 μA mM^{-1} cm^{-2}, the fast response time of 3 s, the linear range of 0.01 to 8 mM, and low determination of 0.7 μM limit have made this sensor one of the most well-planned glucose sensors in the literature.[28−31] In a recent study, we showed that surface assisted (SurfAst) urethane polymerization had enabled height control in nanometer precision.[32] SurfAst urethane polymerization yields a thin polyurethane (PU) interface and does not require inert conditions, degassing, or even high-cost catalysts that limit the feasibility. We utilized this promising modification technique as a new rLBL methodology. In this study we describe a strategy to build up a nanometer-thick gel on an isocyanate functionalized gold surface by the aza-Michael addition reaction of a triple bond containing polyester (PE) and branched polyethylenimine (BPEI). The nanogel coating is formed by an rLBL assembly of BPEI and PE on a gold surface. rLBL is generated by the rapid condensation reaction of the alkyne group of PE and $-NH_2$ groups of BPEI by yielding a homogeneous gel coating on the gold substrate. The key aspect of the described methods is to use aliphatic diisocyanate which offers a powerful alternative to thiol chemistry used in the gold surface functionalization. The soft biointerface obtained by the described methodology may potentially exhibit three major advantages over the common methods: (i) The use of diisocyanate is a faster and more powerful alternative to gold−thiol chemistry. For example, 24 h incubation time is suggested for gold−thiol assembly, whereas the current methodology requires less than 30 min for functionalization. (ii) LBL and most rLBL structures yielded on the surface by solvent exclusion, whereas the described method provides a gel coating that facilitates mass and electron transfer toward the electrode. Therefore, the nanogel coating provides a stable and soft 3D structure on the surface with a large surface area, for biosensor systems. (iii) The third advantage of the current method is the pre- or post-functionalization possibility of gel coating. It could be readily acquired to respond rapidly to many of the target analytes through rapid ion and electron movement. We foresee that the nanogel characteristic may spare distance between reacting multilayers and provide openings in a network that facilitate the transfer of charge and matter. The redox-active rLbL nanogel was obtained by ferrocene attachment to the polyethylenimine (BPEI (Fc-BPEI)) and thus the rLbL nanogel was turned into a nondiffusive electron mediator.[33,34] This soft biointerface may be desirable for bioamperometric-type glucose sensors,[27,28,33] since it is electroactive and allows mass transfer due to the gel network. The 3D structure of the rLbL may potentially be a scaffold for multilayer enzyme immobilization on electrodes useful for cascade reactions.[28] On the other hand, amino-terminated surfaces show good results in cell adhesion,[35] protein adsorption,[36] DNA immobilization,[37] and enzyme loading capability as a biointerface.[34] The rLbL nanogel is considerably homogeneous as generated on the gold surface and allows electron transfer. Also, the surface charge of the rLbL nanogel controls the electrostatic interactions and adsorptions with other biomolecules such as redox proteins. Thus, the surface characteristic of the rLbL promises functionalizations from the acidic to neutral bulk solution medium.[38,39] The presence of the ferrocene groups not only on the outer layer but also within the three-dimensional structure is provided by every layer on the gold surface. The electroactive nanogel interface on the gold surface increases the surface activity to the immobilized structures with adjustable morphology. We present here, a high precision in thickness control of a gel made of the aza- Michael addition reaction of PE and BPEI that shows that good permeability. These results promise the use of nanogel as a coating film, and rLBL films having nanogel characteristics exhibit potential for the promising applications of a soft biointerface.

MATERIALS AND METHODS

Materials. 11-Mercapto-1-undecanol, hexamethylene diisocyanate (HDI), dibutyltin dilaurate 95% (DBTDL), branched polyethylenimine (BPEI) (Mw: 25000), ferrocene carboxaldehyde 98%, acetone, ethanol, and chloroform were purchased from Sigma-Aldrich and used as received without further purification. Polyester (PE) was synthesized as described elsewhere.[40]

Infrared measurements were carried out by using a PerkinElmer Spectrum 100 FT-IR with VeeMAX III Variable Angle Specular Reflectance Accessory at 45° angle reflectance in a spectral range between 1000 and 3600 cm^{-1} to observe functional groups of nanogels on gold surfaces. Nanosurf AFM (Stat0.2LAuD, static force) was used for the topographical characterization of gold surfaces. To investigate electrostatic properties electrostatic force microscopy (EFM) measurements were applied with a double-pass mode by 40 nm height at room temperature. The electrically conductive probes which were purchased from Budget Sensor: Electri-TAP 150-G, ElectriCont-G, and ElectriMulti 75-G were used for both AFM and EFM analysis. Cyclic voltammetry (CV) and electrochemical impedance spectroscopy (EIS) experiments were performed using a Gamry REF600 potentiostat/galvanostat. As working electrodes, nanogel functionalized gold surfaces were used. All electrode potentials cited in this work were measured against Ag/AgCl (saturated KCl), and the counter electrode was a platinum wire at room temperature. As an electrolyte solution, 0.01 M phosphate buffer with 1 mM $K_4Fe(CN)_6$ solution was used. Previous to the measurements, aqueous solutions were deoxygenated by bubbling nitrogen. Impedance spectra in the range 10^5−10^{-1} Hz were recorded with 10 mV/rms amplitude potential perturbation. XPS point analysis was performed at a pass energy of 30 eV. An Al Kα monochromatic (1486.68 eV) beam was used with a spot size of 50 μm (3 number of scans).

Functionalization of the Surface. Gold substrates were cleaned by the RCA cleaning process in order to remove the organic impurities. RCA cleaning solutions contained water (DI), 30% hydrogen peroxide, and 27% ammonium hydroxide (5:1:1 per volume)), and the procedure takes place at 80 °C for 30 min. Gold surfaces were rinsed with excess DI water and dried by N2 blowing.

https://doi.org/10.1021/acs.langmuir.1c01070
Langmuir 2021, 37, 10902−10913

Scheme 1. Schematic Representation of Nanogel Formation Using the rLBL Assembly Method on the Gold Surface[a]

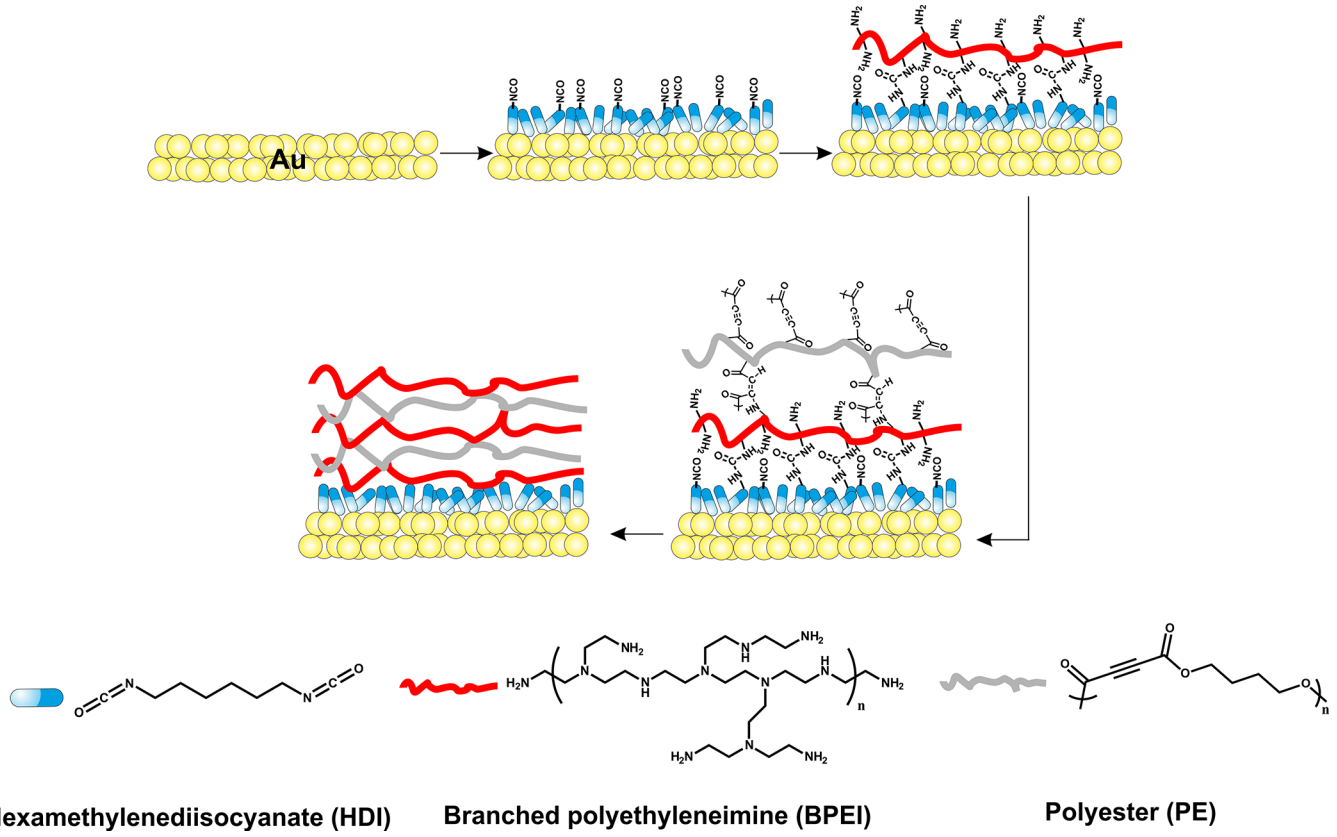

[a]The gold surface was incubated with HDI monomer; hence, the surface is functionalized with isocyanate groups. The 6-multilayered rLBL assembly of BPEI and PE with a triple bond on the isocyanate functionalized gold surface, respectively, gives a high yield nanogel structure on the gold surface.

The gold substrate passivation was applied by using 11-mercapto-1-undecanol. A polydimethylsiloxane (soft lithography—PDMS) stamp was incubated in 1 mM 11-mercapto-1-undecanol in an ethanolic solution for 5 min, and the stamp was dried by a jet of nitrogen gas. Then, the stamp was placed on the gold substrate by applying slight pressure to ensure good contact between the PDMS and the surface.[41]

HDI (0.174 M) solution was prepared in 2.5 mL of acetone, and DBTDL (0.09 mM) was used as a catalyst. Prior to rLBL assembly, the gold surface was precondition by incubating in HDI solution at 40 °C for 30 min. After incubation, the gold was sonicated with chloroform. Then, as the polymer grafting process, the gold substrate was incubated with 0.0012 M BPEI solution in chloroform at 40 °C for 30 min, and the gold surface was cleaned through sonication with chloroform to remove excess polymers. After sonication, the gold substrate was incubated in 0.0034 M PE solution in chloroform at room temperature for 30 min. At the end of the incubation, the gold surface was cleaned through sonication with excess chloroform. Four further layers are obtained by rLBL assembly with BPEI and PE incubation steps, respectively.

The branched polyethylenimine modified with ferrocene carboxaldehyde (Fc-BPEI) was synthesized as described elsewhere.[42] According to the ferrocene carboxaldehyde amount, 10% Fc-BPEI was synthesized. The yield of modified Fc-BPEI was obtained by NMR (Figure SI1). The electroactive nanogel was obtained using equimolar Fc-BPEI instead of BPEI during the reactive layer-by-layer as described above.

In Scheme 1 the nanogel structure has been illustrated to be fabricated using rLBL assembly with BPEI and polyester with a triple bond (PE) on the isocyanate functionalized gold surface. In our previous study, it was demonstrated by X-ray photoelectron spectroscopy (XPS) and density functional theory (DFT) methods that HDI interacts with the gold surface under certain conditions, and the surface is initiated with isocyanate groups.[32] After the surface is activated with isocyanate groups in the first step, the gold surface is incubated with BPEI in the second step. The BPEI has been grafted onto the surface thanks to the formation of urea groups between the gold surface which has free isocyanate groups and amine groups of BPEI. In the third step, the BPEI grafted surface is incubated with a polyester which has an internal electron-deficient triple bond (PE). Meanwhile, PE gives an aza-Michael addition reaction (amino−yne reactions) using primary amines of BPEI, and the reacted triple bonds form a double bond; thus, PE is grafted onto the gold surface.[43] By rLBL assembly of BPEI and PE, respectively, the grafting forms a nanogel on the gold surface. At the end of the sixth step, a nanogel form containing NH_2 groups, double bonds, and triple bonds is obtained, which can yield a postfunctionalizable interface on the gold surface.

RESULTS AND DISCUSSION

The light microscope images shown in Figure 1a demonstrated that the reactive assembly of PE−PEI had led to form a homogeneous film and smooth coverage in a large area (1 cm^2) provided by six sequential steps of reaction on the gold surface (six-multilayered rLBL). The dark and bright features were found to be evenly distributed over the gold substrate. The two desired properties of the homogeneous coating and good electron transfer capability are found to be optimum in six-multilayers rLbL coating. Therefore, six-multilayer rLbL was studied more in detail both in surface and electrochemical characterization.

AFM imaging in Figure 1b,c shows the height difference between the dark and bright features, and the cross-section

https://doi.org/10.1021/acs.langmuir.1c01070
Langmuir 2021, 37, 10902−10913

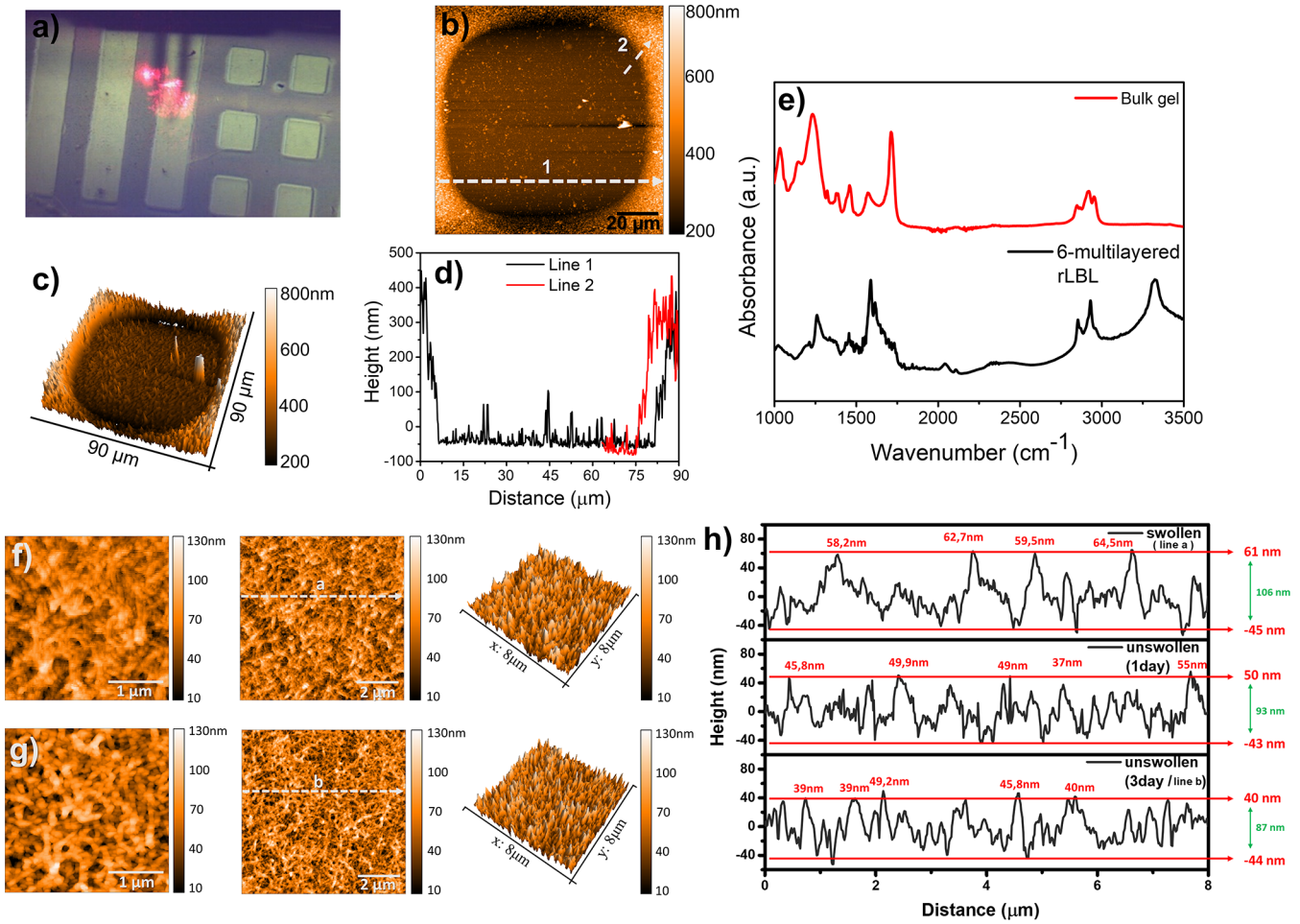

Figure 1. Six-multilayered rLBL gold surface, (the square region was passivized with 11-mercapto-1-undecanol): (a) microscope image, (b) AFM topography image, (c) 3D chart view of panel a, (d) cross-section of white dashed lines 1 and 2, respectively, (e) FT-IR spectrum of bulk gel and six-multilayered rLBL nanogel coated gold surface, and six-multilayered rLBL gold surface without any passivation; (f) AFM topography images right after coating (swollen) (g) AFM topography images after 3 days from the coating (nonswollen), (h) cross-section of the swollen and unswollen surface. (After 1 and 3 days in the room conditions for air-dry, lines were taken from the considered same region from the sample, respectively.)

analysis proved that the average height is about 370 ± 60 nm for rLBL films of PE−PEI upon six-multilayered rLBL (additional analysis shown in Figures SI2 and SI3). In Figure 1b, the square region is passivated by using 11-mercapto-1-undecanol. rLBL formation occurs in the nonpassivated area; therefore, the difference at the edge of the squares yields precisely the thickness of the six-multilayered rLBL. The height/distance plot (Figure 1d) corresponds to the thickness difference between the gold surface and nanogel regions. It shows that the six-multilayered rLBL films favor cumulative deposition over the entire surface rather than separate random agglomeration. rLBL films after six-multilayered rLBL reactions exhibit roughness of 50 nm over 8 μm (see Figure 1h). The calculated roughness is found to be similar to an earlier report of El Haitami et al. (230 nm ±57 nm) that describes the covalent assembly of ethylene glycol functionalized poly-(acrylic acid) by homobifunctional spacers via alkyne and azide reaction.[44] In another study a multilayer coating of elastin-like recombinamers via Huisgen 1,3-dipolar cycloaddition of azides and alkynes, exhibited a surface roughness varying between 20 and 70 nm.[45] These results indicate that rLBL films of PE and PEI via an aza-Michael addition reaction exhibit similar coating properties with a click-type of covalent LBL techniques. Further AFM characterization shown in Figure 1f revealed that the swollen (with chloroform) rLBL films exhibit unstructured and smoother topography as compared to the unswollen (without chloroform) form (see Figure 1g). In addition, in Figure 1 panels f and g the passivation with 11-mercapto-1-undecanol was not applied on the gold surface and the six-multilayered rLbL nanogel structural behavior of swollen and unswollen was examined on the entire gold surface. The surface area roughness is calculated from the area of the maximum profile peak height of the line. The surface area roughness of 9 μm^2 of the swollen six-multilayered rLBL was found to be 63 nm, while the unswollen six-multilayered rLBL was found to be 74 nm. It is expected that the removal of chloroform from the rLBL film network eventually generates protrusions and indentations which increase the roughness of the surface. The profile analysis shown in Figure 1h assures that the number of protrusions per unit distance increased by drying as compared to that seen with the swollen (chloroform loaded) form of rLBL films. The figure shows the cross sections graphs demonstrating the height difference between the protrusions and indentations. Overall the minimum points (indentations) remain similar, but the maximum height changed between the 1 and 3 days left to solvent evaporation.

https://doi.org/10.1021/acs.langmuir.1c01070
Langmuir 2021, 37, 10902−10913

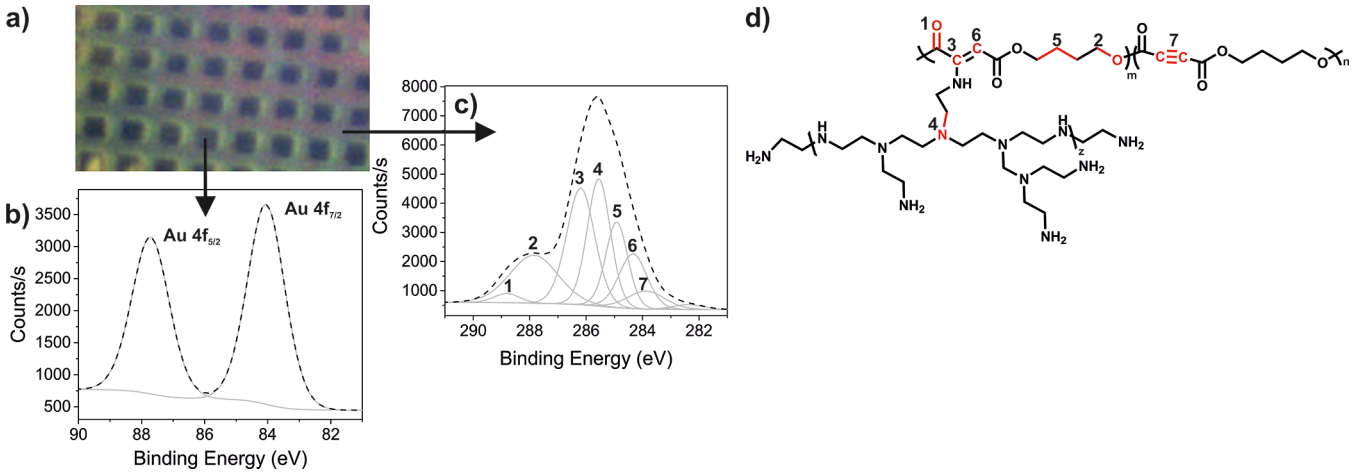

Figure 2. (a) Light microscope image after six-multilayered rLBL; (b) XPS spectra of Au 4f (inside square); (c) XPS spectra of C 1s (polymer region); (d) chemical scheme corresponding to XPS spectra of panel c.

Significant differences in swollen and unswollen surface heights were seen, as seen in the height/distance plot 3 days later. The height difference between the protrusions and indentations is around 106 nm in the swollen rLbL while it is 87 nm in the unswollen rLbL. However, the unswollen rLbL surface has more protrusion and indentations per unit distance specifically. Thus, surface roughness was considered to be increased with the number of indentations by the loss of the solvent. To obtain statistically reliable roughness, we have conducted cross-section analysis from several lines shown in Figure SI4. The figure shows that iterative cross-section lines are more scattered along the *z* axis for unswollen samples as compared to swollen samples. The area roughness was found to be 20% larger for unswollen samples. Therefore, we concluded that the area roughness increases significantly by solvent evaporation. These results refer to the swelling of rLBL films by chloroform and the organogel characteristic of rLBL films of PE−PEI. Overall, the swollen form of the rLBL films of PE and PEI exhibits high height profiles as compared to dried films, and as solvent molecules are removed from the film, height decreases while increasing roughness as a consequence of the collapse of the rLBL film by chloroform removal. The FTIR spectrum of PE-BPEI bulk gel and rLBL film on the gold surface is illustrated in Figure 1e. The rLBL films exhibit the ester conjugated internal alkyne chain triple bond (C≡C) stretching observed at 2046 and 2112 cm^{-1} while the bulk gel did not exhibit substantial peaks at the same region. It may be attributed to the remaining unreacted alkyne chain triple bond (C≡C) in the rLBL film. Both bulk gel and rLBL films exhibited a C−O−C asymmetric stretching vibration of ester occuring at 1261 cm^{-1} and symmetric stretching vibration occurs at 1023 cm^{-1}. Upon the addition reaction, the broad and unstructured absorption signal at 1616 cm^{-1} corresponds to C═C conjugated with C═O (see also Figure SI5 for Raman spectra). These stretching vibrations demonstrate that not all alkyne chains give an addition reaction, and as the layer number increases, the double bond formation increases as a result of the reaction. Also, the C−H stretching vibrations occur at around 2933−2857 cm^{-1} and C−H bending at 1456 cm^{-1}. The strong absorption band at 1588 cm^{-1} is attributed to the N−H bending vibration of amines, while N−H stretching occurs at 3332 cm^{-1}. Michael addition resulted in increased secondary amine peak intensity overlaps with free amine groups in the BPEI. The FTIR spectrum showed that PE readily underwent an aza-Michael addition reaction with BPEI chains on the surface, keeping some triple bonds unreacted, thereby facilitating postfunctionalization.[46−48]

Figure 2a shows a microscope image of mesh patterned PE−PEI gel provided by six-multilayered rLBL, and black arrows point out gold (dark) and polymer (bright) regions where XPS point analyses have been performed. Figure 2b demonstrates the XPS spectra of Au 4f that corresponds to the position of the Au 4f5/2 peak at 87.71 eV and Au 4f7/2 peak at 84.08 eV. The C 1s spectrum, as shown in Figure 2c, was deconvoluted into seven peaks. The peak at 288.43 eV (fwhm, 1.57) and 287.61 eV (fwhm, 1.14) corresponds to the **C**═O (**1**) PE and **C**−O (**2**) groups of polyester. The binding energy of 286.26 eV is the most important peak, corresponding to the reaction of PE and BPEI on the gold surface. Earlier, González-Torres reported an XPS study about the structure of a union of three pyrrole and three ethylene glycol molecules that indicate 286.39 eV attributed C═CN−C states which are the bonds of Py−Py.[49] The bond formed after the reaction between PE and PEI may be similar to the growth of polypyrroles; therefore, the binding energy of C═**C**−N−C (**3**) could be assigned to 286.26 eV (fwhm, 1.39).[50,51] The peak located at 285.49 eV (fwhm, 1.18) and 284.08 eV (fwhm, 0.92) can be attributed to **C**−N (**4**) and C═**C**H−C (**6**) groups.[52] Also, the binding energy peak of the C−N bond is significant since the bond solely originates from the BPEI. The peak at 283.33 eV (fwhm, 0.79) and 284.77 eV (fwhm, 1.01) corresponds to C≡C (**7**) triple bonds and C−C (**5**) aliphatic carbons.[53] These XPS results show that the rLBL assembly forms by reacting BPEI and PE polymers on the gold surface. The XPS depth profiling analysis is used as an analysis method for revealing the chemical composition and internal structure of layer-by-layer thin films.[54−56] Recently, Taketa reported the nanostructured coatings of electrostatic interactions of chitosan (CHI), carboxymethylcellulose (CMC), and sodium polystyrene sulfonate (PSS) as PSS/CHI and CMC/CHI model systems on silicon substrate by depth profiling XPS analysis. The internal structure of the LBL films was well described especially in terms of thickness/cycle (nm) for the ratio of the polymer in the study.[57] Therefore, XPS depth profiling analysis was performed to find out the average thickness of each layer of the rLBL assembly and to investigate

https://doi.org/10.1021/acs.langmuir.1c01070
Langmuir 2021, 37, 10902−10913

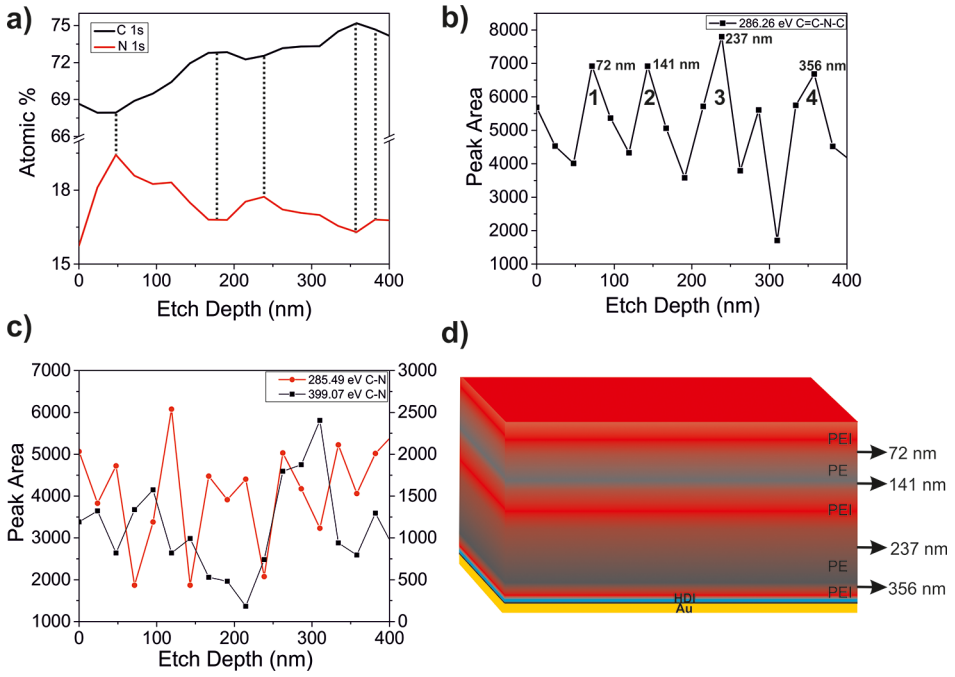

Figure 3. (a) Atomic percentage of carbon and nitrogen with increasing etch depth on the gold surface; (b) etch depth versus peak area of 286.26 eV (C═**C**−N−C); (c) etch depth versus peak area of 285.49 eV (**C**−N) and 399.07 (C−**N**) eV; (d) schematic of XPS depth profiling results of six-multilayered rLBL assembly.

homogeneity. The change of the atomic percentage of nitrogen and carbon values due to increased depth is shown in Figure 3a. A nitrogen abundancy curve (red trace), exhibits two semicircular downward-slope trend while the carbon abundancy curve (black trace), shows two semicircular upward-slope shapes. The first peak at around 48 nm in percent nitrogen was associated with the most intense point of BPEI corresponding to the sixth layer. The nitrogen percentage decreases beyond 50 nm depth while increase in carbon percentage. The first maximum in carbon percentage was found to be around 170 nm associated to the fifth layer, and the nitrogen percentage was relatively low. The local maximum in nitrogen percentage was observed at around 240 nm which corresponded to the fourth layer. As expected, the carbon percentage reached another local maximum at 350 nm by the deeper etching. This level of height was associated to the third layer of consecutive reactions. The last peak of the nitrogen percent related to the second layer was determined at 390 nm. The C═**C**−N−C bond formed by the reaction of PE and BPEI has a binding energy corresponding to 286.26 eV and Figure 3b shows the peak area corresponding to the etch depth at 286.26 eV. In this figure, the peak points at 72 nm 141 nm, 237 nm, and 356 nm may indicate an interface between PE and BPEI (the peaks points attributed to the transition point between the polymers). We therefore assumed that there is a constant thickness increase for consecutive layers rather than significant variations; however, consecutive layers may marginally exhibit thickness differences due to the varying extent of solvent in the layers. It is assumed that the thickness of the resultant rLBL film could be controlled depending on the incubation time and polymer concentration and incubation temperature. In this study, 30 min of incubation time was applied to completely saturate the gold surface, though the reaction between PE and PEI occurs much faster. However, the variations in incubation time and concentration as well as incubation temperature have to be considered as important parameters for thickness control. Taketa et al. presented XPS depth profiling of LBL films made of chitosan-PSS and chitosan-carboxymethyl cellulose exhibiting a constant thickness increase between consecutive layers. They also concluded that the molecular weight of polymers involving LBL and the degree of acetylation (available reactive sites) are critical for the formation of LBL as well as thickness control.[57]

Figure 3c shows the peak areas of binding energy 285.49 eV (**C**−N) and 399.07 eV (C−**N**) corresponding to etch depth. Peak areas of 285.49 and 399.07 eV have similar up/downs and correlations as the etch depth changes. Figure 3d, depicts XPS depth profiling analysis schematically which has been sketched based on the C═**C**−N−C peak intensity from Figure 3b. As indicated, rLBL films were condensing due to the interfacial reaction of PE with Aza-Michael addition and accumulating on top of each other, thereby generating PE and BPEI rich layers. The yield of the rLBL reaction was determined by the ratio of the binding energy field at 286.26 eV corresponding to the C═CN−C bond and 283.33 eV corresponding to the C≡C triple bond. The average of the (from the top to 400 nm) area values of 286.26 and 283.33 eV ratio with increasing etch depth shows that 86.4% of the carbon triple bonds of PE reacted with BPEI while 13.6% remained unreacted. Also, these results are consistent with the FT-IR spectrum peaks (see Figure 1e).

Electrostatic force microscopy (EFM) was used to determine the stored charge and local electrostatic properties stored by using the polarity of the rLBL films at atmospheric pressure. Considering the differentiation of phase to the tip voltage graph of the nanogel and gold surface, the tip voltage was chosen as ±3 V, and also the tip voltage of 0 V was carried out for reference EFM measurement. All EFM measurement was conducted in double-pass mode with 40 nm second tip lift. Figure 4a shows the phase image obtained when −3, 0, and +3

https://doi.org/10.1021/acs.langmuir.1c01070
Langmuir 2021, 37, 10902−10913

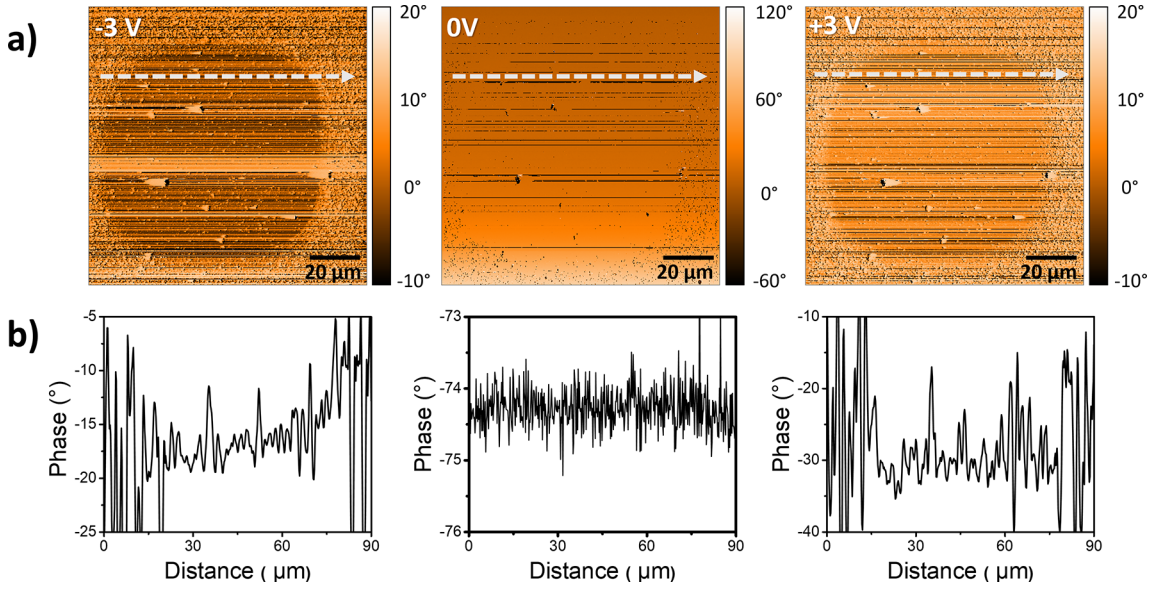

Figure 4. (a) EFM image after six-multilayered rLBL form with −3, 0, and +3 V, respectively; (b) phase shift profiles. (Multi75E-G).

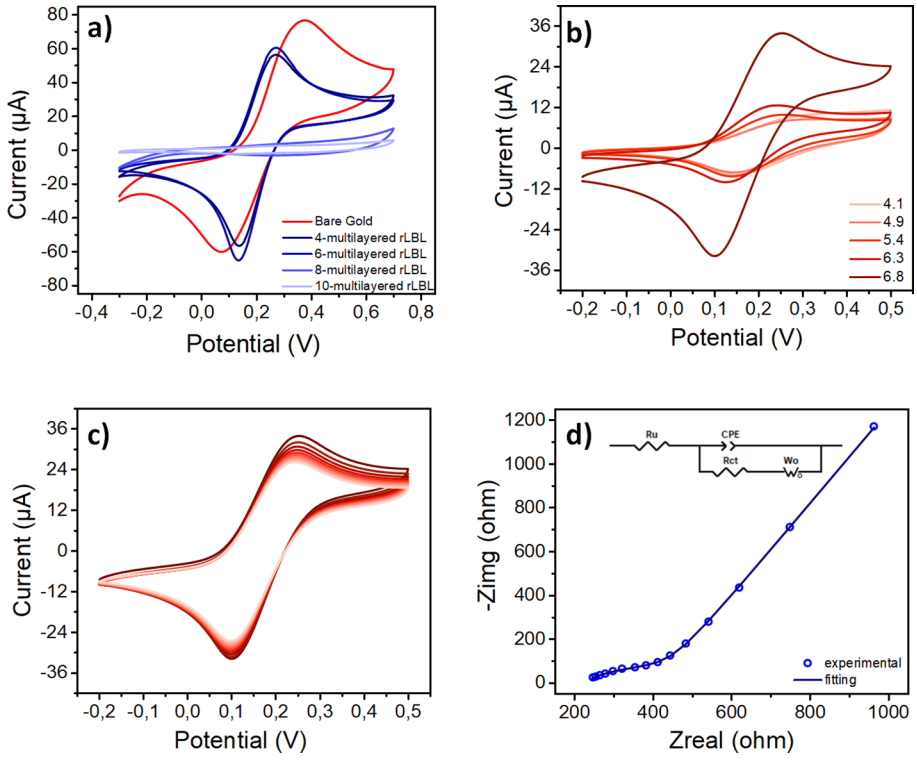

Figure 5. Cyclic voltammograms of (a) bare gold electrode and polymer grafted gold electrodes with variable layers, (b) six-multilayered rLBL gold surface at different pH mediums, (c) 6-multilayered rLBL gold surface sequential 10 scanning potential cycles at 6.8 pH, at 50 mV/s in the presence of 1 mM $K_4[Fe(CN)_6]$ in 0.01 M PBS, and (d) Nyquist's plot of six-multilayered rLBL gold surface in the presence of 1 mM $K_4[Fe(CN)_6]$ at 0.01 M PBS solution at pH 6.8.

V are applied to the tip, respectively. There was a contrast differentiation prominently at +3 and −3 V between the polymer and the gold layer; however, the entire surface showed the identical behavior at 0 V. According to the phase image, Figure 4b shows the phase shift obtained when −3, 0, and +3 V are applied to the tip, respectively. Upon −3 V application to the tip, the phase shift was 15 degrees between the nanogel and gold layer, and when +3 V is applied a 20 degrees shift was observed. These results demonstrate that the +3 V charged tip tends to interact more with the nanogel on the gold surface than the −3 V. In addition, results may indicate that the +3 V reduce the effective resonance frequency, and the capacitive electrostatic force becomes higher on the nanogel.[58,59]

The electrochemical characterizaiton of rLBL was performed by cyclic voltammetry in a 0.01 M phosphate buffer solution containing 1 mM $K_4[Fe(CN)_6]$ (potassium ferrocyanide) as a redox probe. The potential range is 0.7 to −0.3 V with a scanning speed of 50 mV/s. The bare gold surface cyclic

https://doi.org/10.1021/acs.langmuir.1c01070
Langmuir 2021, 37, 10902−10913

voltammogram was examined in the same conditions in order to show unmodified surface characteristics. Cyclic voltammograms for rLBL films with different numbers of layers and bare gold surfaces were presented in Figure 5a. According to a reactive multilayer polymer coating, the effect of the thickness on the surface to the electron transfer was investigated. The formal redox potential of the reaction is directly relevant to the surface coating thickness. Generally, the increasing hydrocarbon chain length and denser orientation will increase the peak separations and redox potentials, and decrease the peak currents.[60−62] So, every assembled layer suppresses the faradaic processes such as electron transfer. The peak currents after four-multilayered rLBL and six-multilayered rLBL were gradually decreased, which shows the polymer layers were successfully coated on the gold electrode. Although the polymer film did not completely block electron transfer, relatively small peak currents were an indication of a rather slow electron transfer. However, the six-multilayered rLBL film coated electrode had a slightly great cathodic peak current. Hence, the reduction of the ferricyanide takes place easily as compared to the four-multilayered rLBL since six-multilayered rLBL films provide a greater extent of surface coverage rather than nonorientated aggregates. Additionally, the anodic peak potentials shift to more negative values and cathodic peak potentials shift to slightly more positive values by approximately 110 mV and 70 mV, respectively. The rLBL coated surfaces have a relatively small peak current and narrow peak-to-peak separation than the bare gold surface. The narrow peak-to-peak shows rLBL coated surfaces beneficial to increase the electrochemical reversibility of the redox couple on the electrode.[62] In both cases, four-multilayered rLBL, and six-multilayered rLBL cyclic voltammograms exhibit quasi-reversible properties that indicate redox probe diffuses and electron transfer occurs at the electrode surface. The rLBL formal redox potential slightly lower than that of bare gold shows the rLBL surface coating has a positive effect on the redox energy barrier up to six-multilayered rLBL.[62] Additionally, four-multilayered rLBL and six-multilayered rLBL formal redox potentials and peak-to-peak separations remain similar to each other showing that rLBL retains its redox properties. The increased number of polymer coated layers and densely packed hydrocarbon structures lead to peak broadening and a decrease in peak currents. So, the number of hexacyanoferrate ions reaching the electrode surface is restricted and plateau-shaped current characteristics occur.[60,63,64] For this reason, the surface thickness directly affects the electron transfer of the soluble species and essentially blocks the ion migration at eight-multilayered and 10-multilayered rLBL coated gold surfaces. Hence, six-multilayered rLBL coated gold was selected to investigate and develop the surface properties due to its relatively high peak currents and narrow peak separation. The effect of pH on a six-multilayered rLBL film coated electrode was studied by cyclic voltammetry in a 0.01 M phosphate buffer with 1 mM $K_4[Fe(CN)_6]$. Figure 5b shows the cyclic voltammogram of the six-multilayered rLBL coated surface in media with various pH values. The pH change was examined from 6.8 to 4.1 because the protonation degree of the amine groups increased with the acidity, and the rate of electron transfer depending on the acidity of the medium has been investigated. As shown in Figure 5b, the peak-to-peak separation and peak currents are decreased by increasing the acidity from a neutral to an acidic environment. This result may arise from the protonation of amine tail groups and the negatively charged separation of the polyester polymer on the electrode surface. Previous studies showed the isoelectric point of the pristine polyester fibers at pH 4.0.[65,66] At pH values below 4.0, the polyester was positively charged, and the zeta potential in the plateau region of the polyester was found to be −39 mV in an ionic solution of 10^{-3} M KCl, while it was recorded as −30 mV at pH 7.0.[66] On the other hand, the PEI zeta potential obtained a plateau value at pH < 6 nearby 70/90 mV for an $10^{-2}/10^{-3}$ M ionic strength of NaCl.[67] Also, PEI was found to be effectively charged (protonated) 30% to 70% from pH 7.0 to pH 3.0.[67] Mészáros et al. reported that PEI is completely uncharged at pH ≥ 10.5.[68] Earlier Marmiosollé et al., investigated the electrochemical response of the NH_2 terminated SAM surface resembling PEI. They reported that the CV peak separations of amine-terminated SAMs decreased, and peak currents increased as the solution pH was lowered from 5.18 to 3.16.[69] The reason was that the protonation degree of the amine groups increased with the acidity, and therefore the SAMs became less compact, which facilitated electron transfer. It seems that a six-multilayered rLBL coated surface exhibited a decrease in peak-to-peak separation and peak currents as pH decreased. This result may occur because the PE is uncharged at pH 4.1 and PEI has greater zeta potential compared to the PE at neutral medium. So, at pH 6.8, the electrostatic attraction between PEI and PE may generate positive charges at the surface due to the charge separation. This behavior indicates that the probe diffuses more freely through the layer and undergoes electron transfer at the electrode surface in a neutral medium as compared to in an acidic medium. On the other hand, increasing the acidity of the medium restricted the rate of the electron transfer but did not block it completely.

Figure 5c shows cyclic voltammetry of a 6-multilayered rLBL coated surface at pH 6.8 for 10 cycles. The anodic and cathodic peak potentials were observed relatively constant at 0.27 and 0.14 V, respectively, although the electro-generated ferricyanide ions reduction is faster than oxidation of ferrocyanide ions when the pH is 6.8. In addition, the electrochemical response exhibited instability such that the current response decreased with each subsequent scan. So, the percent decrease in the primary oxidation was 20.7%, after a 10-cycle operation, whereas the primary reduction peak percent decrease was 15% .[69] Electrochemical impedance spectra were taken at 0 V and in the 10^5-10^{-1} Hz frequency range. The Nyquist representation of a six-multilayered rLBL coated gold surface is shown in Figure 5d. EIS spectra was fitted to a Randles circuit which consisted of a constant phase element (CPE), parallel connected charge transfer resistance (Rct), and a series connected open Warburg element (Wo); all in series with the active electrolyte resistance (Rsol). The incomplete semicircle in the Nyquist plot corresponded to capacitive behavior. The effective capacitance from the constant phase element and resistance of charge transfer was calculated as $C_{eff.} = [QR^{(1-\alpha)}]^{1/\alpha}$. The capacitance of the six-multilayered rLBL polymer grafted gold surface was found as 0.2736 Farad. This result assures that the rLBL film exhibits certain property for charge accumulation in aqueous media and may serve as an electroactive coating.

To show a broad range of applicability of rLBL films, we implemented additional modifications on BPEI to utilize as a redox polymer.[70] The high density of the amines in the BPEI backbone allows easy modification of the polymer. Therefore, a redox polymer was produced by attaching ferrocene carbox-

https://doi.org/10.1021/acs.langmuir.1c01070
Langmuir 2021, 37, 10902−10913

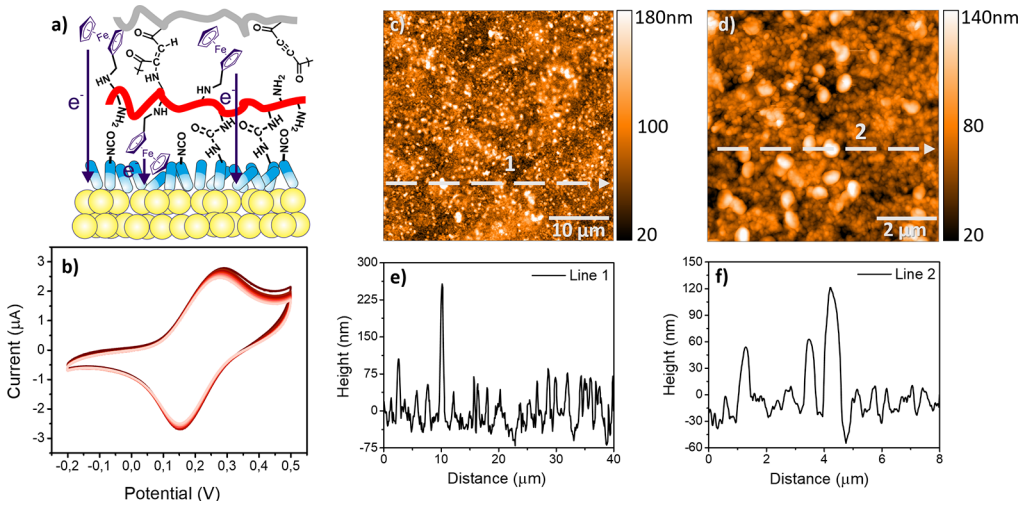

Figure 6. (a) Scheme of Fc-BPEI; (b) CV at 10 mV/s in 0.01 M PBS that did not include $Fe(CN)_6$ at pH 6.8; (c,d) AFM topography images of six-multilayered rLBL gold electrode (ElectriCont-G), Fc-BPEI was used; (e,f) cross-section of white dashed line in panels c and d, respectively.

aldehyde (Fc) redox centers to the BPEI backbone. While the redox polymer generates, the majority of the amino groups remain unsubstituted to enable rLBL assembly with the polyester.[42,71,72] A similar rLBL film formation was performed between PE and Fc-modified BPEI thereby providing an intrinsic electroactive property. Figure 6a shows an illustration of the surface-anchored ferrocene redox center-based layer-by-layer coated gold surface. The cyclic voltammogram in Figure 6b shows the electroactivity of the rLBL films without free Fc in the electrolyte. It confirms that the covalent attachment of Fc to the BPEI provides efficient electron transfer between multilayers without requiring a free redox couple as a mediator. The anodic peak current is 2.6 μA while the cathodic peak current is 1.5 μA. The high density of electron-donating amine groups in the BPEI and weak electron-withdrawing polyester groups in the rLBL increase the rate of the reaction. Hence, easy and fast oxidation behavior of ferrocene was observed. Also, the anodic and cathodic peak potentials were observed at 0.286 and 0.155 V. The electroactive rLBL surface peak-to-peak separation was quite similar to six-multilayered rLBL, which confirms ferrocene modifying was not affecting reversibility.[72]

Figure 6 panels c and d show the AFM results of electroactive nanogel on the gold surface that was formed by using Fc-BPEI and Pe. AFM results showed that there are large aggregates and cloudy-like globular structures forming a homogeneous polymer domain on the surface, and the homogeneity of the polymer regions is lower than that of the surface prepared by using BPEI (Figure 6c). This inhomogeneous structure can be interpreted by the decrease in the number of functional groups of NH_2 on Fc-BPEI that react with PE. Figure 6 panels e and f represent cross-section results of the electroactive nanogel and large aggregates nearly 5 times higher in elevation than the cloudy-like globular structure formed by the homogeneous polymer. The result of the roughness test of 25 μm^2 is nearly 130 nm, and it can be concluded that a smoother surface is obtained by using Fc-BPEI.

CONCLUSION

The rLBL film formation of PE and BPEI via aza-Michael addition reaction has been demonstrated. rLBL films exhibit an organogel-type behavior, providing a solvent associated network and swelling−shrinking properties on the solid substrate. This gel characteristic spares distance between reacting multilayers and provides openings in the network that facilitate the transfer of charge and matter. The XPS depth profiling of the rLBL films also showed that alternating layers mostly consisted of covalently reacted groups as well as unreacted functional groups of primary amines (NH_2) and a carbon−carbon triple bond (C≡C) to some extent. This recalls that rLBL films have postfunctionalizable groups remaining. The electroactivity of the rLBL films was studied by voltammetry and impedance spectroscopy showing that nanogel permeability drove electron transfer effectively. The electrochemical characterization of the nanogels ascertains that electron transfer readily occurs in up to six-multilayered rLbL, whereas it is nearly blocked for a higher number of layers. The rLBL films having nanogel characteristics exhibit potential for the promising applications of soft biointerfaces.

ASSOCIATED CONTENT

Supporting Information

The Supporting Information is available free of charge at https://pubs.acs.org/doi/10.1021/acs.langmuir.1c01070.

Additional AFM images, cross-section analysis, Raman microscope image, reaction scheme, and NMR spectroscopy image (PDF)

AUTHOR INFORMATION

Corresponding Author

Ümit Hakan Yıldız − *Department of Chemistry and Department of Polymer Science and Engineering, Izmir Institute of Technology, Izmir 35430, Turkey;* orcid.org/0000-0002-6922-4454; Email: hakanyildiz@iyte.edu.tr; Fax: +90 232 750 7509

Authors

Oyku Yildirimkaraman − *Department of Chemistry, Izmir Institute of Technology, Izmir 35430, Turkey;* orcid.org/0000-0001-5743-6196

Sezer Özenler − *Department of Chemistry, Izmir Institute of Technology, Izmir 35430, Turkey; Department of Chemistry and Pharmacy & Interdisciplinary Center for Molecular*

https://doi.org/10.1021/acs.langmuir.1c01070
Langmuir 2021, 37, 10902−10913

Materials, Friedrich-Alexander Universität Erlangen-Nürnberg, Erlangen D-91058, Germany; orcid.org/0000-0001-6045-7035

Ufuk Saim Gunay − *Department of Chemistry, Istanbul Technical University, Maslak, Istanbul 34469, Turkey;* orcid.org/0000-0002-3085-3763

Hakan Durmaz − *Department of Chemistry, Istanbul Technical University, Maslak, Istanbul 34469, Turkey;* orcid.org/0000-0003-4710-2496

Complete contact information is available at: https://pubs.acs.org/10.1021/acs.langmuir.1c01070

Author Contributions

O.Y.: methodology, investigation, experiment, writing−original draft, writing−review and editing. S.Ö.: conceptualization, methodology, investigation, writing−original draft, writing−review and editing. U.H.Y.: conceptualization, methodology, resources, writing−original draft, writing−review and editing, supervision. U.S.G.: synthesis of a material, review, and editing. H.D.: synthesis of a material, review, and editing.

Notes

The authors declare no competing financial interest.

■ ACKNOWLEDGMENTS

S.Ö. is a YÖK 100/2000 scholarship holder. The authors would like to acknowledge the support of the Scientific and Technological Research Council of Turkey (TUBITAK) 2214-A International Doctoral Research Fellowship Programme for Ph.D. Students. XPS point and depth profiling analysis were performed at Ege University Central Research Testing and Analysis Laboratory Research and Application Center (EGE-MATAL). We are thankful to Dr. Ayşegül Erdoğan for the fruitful discussion of XPS data.

■ ABBREVIATIONS

PE, polyester; BPEI, branched polyethyleneimine; Fc, ferrocene carboxaldehyde; HDI, hexamethylene diisocyanate; PDMS, polydimethylsiloxane; rLBL, reactive layer-by-layer; CV, cyclic voltammetry; EIS, electrochemical impedance spectroscopy; XPS, X-ray photoelectron spectroscopy; AFM, atomic force microscopy; EFM, electrostatic force microscopy; FT-IR, Fourier-transform spectroscopy

■ REFERENCES

(1) An, Q.; Huang, T.; Shi, F. Covalent layer-by-layer films: chemistry, design, and multidisciplinary applications. *Chem. Soc. Rev.* **2018**, *47* (13), 5061−5098.

(2) Richardson, J. J.; Cui, J.; Björnmalm, M.; Braunger, J. A.; Ejima, H.; Caruso, F. Innovation in Layer-by-Layer Assembly. *Chem. Rev.* **2016**, *116* (23), 14828−14867.

(3) Liu, Y.; Bruening, M. L.; Bergbreiter, D. E.; Crooks, R. M. Multilayer dendrimer−polyanhydride composite films on glass, silicon, and gold wafers. *Angew. Chem., Int. Ed. Engl.* **1997**, *36* (19), 2114−2116.

(4) Liu, Y.; Zhao, M.; Bergbreiter, D. E.; Crooks, R. M. pH-switchable, ultrathin permselective membranes prepared from multilayer polymer composites. *J. Am. Chem. Soc.* **1997**, *119* (37), 8720−8721.

(5) Zhao, M.; Liu, Y.; Crooks, R. M.; Bergbreiter, D. E. Preparation of highly impermeable hyperbranched polymer thin-film coatings using dendrimers first as building blocks and then as in situ thermosetting agents. *J. Am. Chem. Soc.* **1999**, *121* (5), 923−930.

(6) Buck, M. E.; Zhang, J.; Lynn, D. M. Layer-by-Layer Assembly of Reactive Ultrathin Films Mediated by Click-Type Reactions of Poly(2-Alkenyl Azlactone)s. *Adv. Mater.* **2007**, *19* (22), 3951−3955.

(7) Such, G. K.; Quinn, J. F.; Quinn, A.; Tjipto, E.; Caruso, F. Assembly of ultrathin polymer multilayer films by click chemistry. *J. Am. Chem. Soc.* **2006**, *128* (29), 9318−9319.

(8) Vestberg, R.; Malkoch, M.; Kade, M.; Wu, P.; Fokin, V. V.; Barry Sharpless, K.; Drockenmuller, E.; Hawker, C. J. Role of architecture and molecular weight in the formation of tailor-made ultrathin multilayers using dendritic macromolecules and click chemistry. *J. Polym. Sci., Part A: Polym. Chem.* **2007**, *45* (14), 2835−2846.

(9) Mamedov, A. A.; Kotov, N. A.; Prato, M.; Guldi, D. M.; Wicksted, J. P.; Hirsch, A. Molecular design of strong single-wall carbon nanotube/polyelectrolyte multilayer composites. *Nat. Mater.* **2002**, *1* (3), 190−194.

(10) Qureshi, S. S.; Zheng, Z.; Sarwar, M. I.; Félix, O.; Decher, G. Nanoprotective layer-by-layer coatings with epoxy components for enhancing abrasion resistance: toward robust multimaterial nanoscale films. *ACS Nano* **2013**, *7* (10), 9336−9344.

(11) Makamba, H.; Hsieh, Y.-Y.; Sung, W.-C.; Chen, S.-H. Stable permanently hydrophilic protein-resistant thin-film coatings on poly (dimethylsiloxane) substrates by electrostatic self-assembly and chemical cross-linking. *Anal. Chem.* **2005**, *77* (13), 3971−3978.

(12) Aumsuwan, N.; Ye, S.-H.; Wagner, W. R.; Urban, M. W. Covalent Attachment of Multilayers on Poly(tetrafluoroethylene) Surfaces. *Langmuir* **2011**, *27* (17), 11106−11110.

(13) Hu, X.; Gong, X. A new route to fabricate biocompatible hydrogels with controlled drug delivery behavior. *J. Colloid Interface Sci.* **2016**, *470*, 62−70.

(14) Ma, L.; Cheng, C.; He, C.; Nie, C.; Deng, J.; Sun, S.; Zhao, C. Substrate-Independent Robust and Heparin-Mimetic Hydrogel Thin Film Coating via Combined LbL Self-Assembly and Mussel-Inspired Post-Cross-linking. *ACS Appl. Mater. Interfaces* **2015**, *7* (47), 26050−26062.

(15) Liu, X.; Wen, N.; Wang, X.; Zheng, Y. Layer-by-Layer Self-Assembled Graphene Multilayer Films via Covalent Bonds for Supercapacitor Electrodes. *Nanomater. Nanotechnol.* **2015**, *5*, 14.

(16) Zhang, S.; Yang, W.; Niu, Y.; Sun, C. Multilayered construction of glucose oxidase and poly(allylamine)ferrocene on gold electrodes by means of layer-by-layer covalent attachment. *Sens. Actuators, B* **2004**, *101* (3), 387−393.

(17) Zhang, S.; Yang, W.; Niu, Y.; Sun, C. Multilayered construction of glucose oxidase on gold electrodes based on layer-by-layer covalent attachment. *Anal. Chim. Acta* **2004**, *523* (2), 209−217.

(18) Sun, Y.; Yan, F.; Yang, W.; Sun, C. Multilayered construction of glucose oxidase and silica nanoparticles on Au electrodes based on layer-by-layer covalent attachment. *Biomaterials* **2006**, *27* (21), 4042−4049.

(19) Olichwer, N.; Leib, E. W.; Halfar, A. H.; Petrov, A.; Vossmeyer, T. Cross-Linked Gold Nanoparticles on Polyethylene: Resistive Responses to Tensile Strain and Vapors. *ACS Appl. Mater. Interfaces* **2012**, *4* (11), 6151−6161.

(20) Ou, X.; Jiang, L.; Chen, P.; Zhu, M.; Hu, W.; Liu, M.; Zhu, J.; Ju, H. Highly Stable Graphene-Based Multilayer Films Immobilized via Covalent Bonds and Their Applications in Organic Field-Effect Transistors. *Adv. Funct. Mater.* **2013**, *23* (19), 2422−2435.

(21) Xiong, Z.; Gu, T.; Wang, X. Self-Assembled Multilayer Films of Sulfonated Graphene and Polystyrene-Based Diazonium Salt as Photo-Cross-Linkable Supercapacitor Electrodes. *Langmuir* **2014**, *30* (2), 522−532.

(22) Guin, T.; Stevens, B.; Krecker, M.; D'Angelo, J.; Humood, M.; Song, Y.; Smith, R.; Polycarpou, A.; Grunlan, J. C. Ultrastrong, Chemically Resistant Reduced Graphene Oxide-based Multilayer Thin Films with Damage Detection Capability. *ACS Appl. Mater. Interfaces* **2016**, *8* (9), 6229−6235.

(23) Li, L.; Shi, Y.; Pan, L.; Shi, Y.; Yu, G. Rational design and applications of conducting polymer hydrogels as electrochemical biosensors. *J. Mater. Chem. B* **2015**, *3* (15), 2920−2930.

(24) Jung, I. Y.; Kim, J. S.; Choi, B. R.; Lee, K.; Lee, H. Hydrogel Based Biosensors for In Vitro Diagnostics of Biochemicals, Proteins, and Genes. *Adv. Healthcare Mater.* **2017**, *6* (12), 1601475.
(25) Karbarz, M.; Mackiewicz, M.; Kaniewska, K.; Marcisz, K.; Stojek, Z. Recent developments in design and functionalization of micro- and nanostructural environmentally-sensitive hydrogels based on N-isopropylacrylamide. *Applied Materials Today* **2017**, *9*, 516−532.
(26) Qu, F.; Zhang, Y.; Rasooly, A.; Yang, M. Electrochemical Biosensing Platform Using Hydrogel Prepared from Ferrocene Modified Amino Acid as Highly Efficient Immobilization Matrix. *Anal. Chem.* **2014**, *86* (2), 973−976.
(27) Freeman, M. H.; Hall, J. R.; Leopold, M. C. Monolayer-Protected Nanoparticle Doped Xerogels as Functional Components of Amperometric Glucose Biosensors. *Anal. Chem.* **2013**, *85* (8), 4057−4065.
(28) Zhai, D.; Liu, B.; Shi, Y.; Pan, L.; Wang, Y.; Li, W.; Zhang, R.; Yu, G. Highly sensitive glucose sensor based on Pt nanoparticle/polyaniline hydrogel heterostructures. *ACS Nano* **2013**, *7* (4), 3540−3546.
(29) Zhou, J.; Liao, C.; Zhang, L.; Wang, Q.; Tian, Y. Molecular Hydrogel-Stabilized Enzyme with Facilitated Electron Transfer for Determination of H2O2 Released from Live Cells. *Anal. Chem.* **2014**, *86* (9), 4395−4401.
(30) Xia, N.; Zhang, Y.; Chang, K.; Gai, X.; Jing, Y.; Li, S.; Liu, L.; Qu, G. Ferrocene-phenylalanine hydrogels for immobilization of acetylcholinesterase and detection of chlorpyrifos. *J. Electroanal. Chem.* **2015**, *746*, 68−74.
(31) Mugo, S. M.; Berg, D.; Bharath, G. Integrated Microcentrifuge Carbon Entrapped Glucose Oxidase Poly (N-Isopropylacrylamide) (pNIPAm) Microgels for Glucose Amperometric Detection. *Anal. Lett.* **2019**, *52* (5), 825−838.
(32) Özenler, S.; Sozen, Y.; Sahin, H.; Yildiz, U. H. Fabrication of a Postfunctionalizable, Biorepellent, Electroactive Polyurethane Interface on a Gold Surface by Surface-Assisted Polymerization. *Langmuir* **2020**, *36* (24), 6828−6836.
(33) Chen, D.; Wang, G.; Li, J. Interfacial Bioelectrochemistry: Fabrication, Properties and Applications of Functional Nanostructured Biointerfaces. *J. Phys. Chem. C* **2007**, *111* (6), 2351−2367.
(34) Milton, R. D.; Wang, T.; Knoche, K. L.; Minteer, S. D. Tailoring Biointerfaces for Electrocatalysis. *Langmuir* **2016**, *32* (10), 2291−2301.
(35) Kuo, C.-W.; Lai, J.-J.; Wei, K. H.; Chen, P. Surface modified gold nanowires for mammalian cell transfection. *Nanotechnology* **2008**, *19* (2), 025103.
(36) Gnanasampanthan, T.; Beyer, C. D.; Yu, W.; Karthäuser, J. F.; Wanka, R.; Spöllmann, S.; Becker, H.-W.; Aldred, N.; Clare, A. S.; Rosenhahn, A. Effect of Multilayer Termination on Nonspecific Protein Adsorption and Antifouling Activity of Alginate-Based Layer-by-Layer Coatings. *Langmuir* **2021**, *37* (19), 5950−5963.
(37) Oh, S. J.; Cho, S. J.; Kim, C. O.; Park, J. W. Characteristics of DNA Microarrays Fabricated on Various Aminosilane Layers. *Langmuir* **2002**, *18* (5), 1764−1769.
(38) Hagemann, A.; Giussi, J. M.; Longo, G. S. Use of pH Gradients in Responsive Polymer Hydrogels for the Separation and Localization of Proteins from Binary Mixtures. *Macromolecules* **2018**, *51* (20), 8205−8216.
(39) Torres, M.; Beppu, M.; Santana, C. Characterization of chemically modified chitosan microspheres as adsorbents using standard proteins (bovine serum albumin and lysozyme). *Braz. J. Chem. Eng.* **2007**, *24*, 325−336.
(40) Cetin, M.; Esen, C.; Daglar, O.; Luleburgaz, S.; Hizal, G.; Durmaz, H.; Tunca, U. 1,3-Dipolar and Diels−Alder cycloaddition reactions on polyester backbones possessing internal electron-deficient alkyne moieties. *Polym. Chem.* **2016**, *7* (46), 7094−7100.
(41) Schneider, M.; Tang, Z.; Richter, M.; Marschelke, C.; Förster, P.; Wegener, E.; Amin, I.; Zimmermann, H.; Scharnweber, D.; Braun, H.-G.; Luxenhofer, R.; Jordan, R. Patterned Polypeptoid Brushes. *Macromol. Biosci.* **2016**, *16* (1), 75−81.
(42) Merchant, S. A.; Glatzhofer, D. T.; Schmidtke, D. W. Effects of electrolyte and pH on the behavior of cross-linked films of ferrocene-modified poly (ethylenimine). *Langmuir* **2007**, *23* (22), 11295−11302.
(43) Gunay, U. S.; Cetin, M.; Daglar, O.; Hizal, G.; Tunca, U.; Durmaz, H. Ultrafast and efficient aza- and thiol-Michael reactions on a polyester scaffold with internal electron deficient triple bonds. *Polym. Chem.* **2018**, *9* (22), 3037−3054.
(44) El Haitami, A. E.; Thomann, J.-S. b.; Jierry, L. c.; Parat, A.; Voegel, J.-C.; Schaaf, P.; Senger, B.; Boulmedais, F.; Frisch, B. t. Covalent Layer-by-Layer Assemblies of Polyelectrolytes and Homobifunctional Spacers. *Langmuir* **2010**, *26* (14), 12351−12357.
(45) Sousa, M. P.; Gonzalez de Torre, I.; Oliveira, M. B.; Rodríguez-Cabello, J. C.; Mano, J. F. Biomimetic click assembled multilayer coatings exhibiting responsive properties. *Materials Today Chemistry* **2017**, *4*, 150−163.
(46) Socrates, G. *Infrared and Raman characteristic group frequencies: tables and charts*, 3rd ed.; John Wiley & Sons: 2004; pp 50−155.
(47) Ford, J.; Marder, S. R.; Yang, S. Growing "nanofruit" textures on photo-crosslinked SU-8 surfaces through layer-by-layer grafting of hyperbranched poly (ethyleneimine). *Chem. Mater.* **2009**, *21* (3), 476−483.
(48) Thompson, J. M. *Infrared Spectroscopy*, 1st ed.; Jenny Stanford Publishing: 2018; p 35−88.
(49) González-Torres, M.; Olayo, M. G.; Cruz, G. J.; Gómez, L. M.; Sánchez-Mendieta, V.; González-Salgado, F. XPS Study of the Chemical Structure of Plasma Biocopolymers of Pyrrole and Ethylene Glycol. *Advances in Chemistry* **2014**, *2014*, 1−8.
(50) Gomez, L. M.; Cruz, G. J.; Olayo, M. G.; Gonzalez-Torres, M.; Gonzalez-Salgado, F.; Lopez-Gracia, O. G. Analysis of crosslinking in polypyrrole particles synthesized by plasma. *Polym. Bull.* **2014**, *71* (12), 3275−3287.
(51) González-Torres, M.; Olayo, M. G.; Gómez, L. M.; Morales, J.; Olayo, R.; Ramírez, R.; Flores, F. G.; Mejía-Cuero, M. R.; Cruz, G. J. Chemical interactions of heparin in porous polypyrrole, an example of drug−carrier destructive interaction. *Polym. Bull.* **2020**, *77* (1), 375−385.
(52) Beamson, G. B. D. High Resolution XPS of Organic Polymers: The Scienta ESCA300 Database (Beamson, G.; Briggs, D.). *J. Chem. Educ.* **1993**, *70* (1), A25.
(53) Rybachuk, M.; Bell, J. M. Electronic states of trans-polyacetylene, poly(p-phenylene vinylene) and sp-hybridised carbon species in amorphous hydrogenated carbon probed by resonant Raman scattering. *Carbon* **2009**, *47* (10), 2481−2490.
(54) Gilbert, J. B.; Rubner, M. F.; Cohen, R. E. Depth-profiling X-ray photoelectron spectroscopy (XPS) analysis of interlayer diffusion in polyelectrolyte multilayers. *Proc. Natl. Acad. Sci. U. S. A.* **2013**, *110* (17), 6651−6656.
(55) Lee, H.; Gilbert, J. B.; Angilè, F. E.; Yang, R.; Lee, D.; Rubner, M. F.; Cohen, R. E. Design and Fabrication of Zwitter-Wettable Nanostructured Films. *ACS Appl. Mater. Interfaces* **2015**, *7* (1), 1004−1011.
(56) Sydow, S.; de Cassan, D.; Hänsch, R.; Gengenbach, T. R.; Easton, C. D.; Thissen, H.; Menzel, H. Layer-by-layer deposition of chitosan nanoparticles as drug-release coatings for PCL nanofibers. *Biomater. Sci.* **2019**, *7* (1), 233−246.
(57) Taketa, T. B.; dos Santos, D. M.; Fiamingo, A.; Vaz, J. M.; Beppu, M. M.; Campana-Filho, S. P.; Cohen, R. E.; Rubner, M. F. Investigation of the Internal Chemical Composition of Chitosan-Based LbL Films by Depth-Profiling X-ray Photoelectron Spectroscopy (XPS) Analysis. *Langmuir* **2018**, *34* (4), 1429−1440.
(58) Lei, C. H.; Das, A.; Elliott, M.; Macdonald, J. E. Quantitative electrostatic force microscopy-phase measurements. *Nanotechnology* **2004**, *15* (5), 627−634.
(59) El Khoury, D. *Towards the use of electrostatic force microscopy to study interphases in nanodielectric materials*. Ph.D. Thesis, Université Montpellier, 2017.
(60) Chou, A.; Eggers, P. K.; Paddon-Row, M. N.; Gooding, J. J. Self-assembled carbon nanotube electrode arrays: effect of length of

https://doi.org/10.1021/acs.langmuir.1c01070
Langmuir 2021, 37, 10902−10913

the linker between nanotubes and electrode. *J. Phys. Chem. C* **2009**, *113* (8), 3203−3211.
(61) Shein, J. B.; Lai, L. M. H.; Eggers, P. K.; Paddon-Row, M. N.; Gooding, J. J. Formation of Efficient Electron Transfer Pathways by Adsorbing Gold Nanoparticles to Self-Assembled Monolayer Modified Electrodes. *Langmuir* **2009**, *25* (18), 11121−11128.
(62) Zheng, Q.; Ding, K.; Huang, X.; Shao, H. Self-assembled monolayer assisted binding of partially oxidized graphene on gold: Tunable electron-transfer mediation and in-situ electrochemical disassembly. *Appl. Surf. Sci.* **2017**, *425*, 188−193.
(63) Finklea, H. O. Self-Assembled Monolayers on Electrodes. *Encyclopedia of Analytical Chemistry* **2006**, No. a5315, DOI: 10.1002/9780470027318.a5315.
(64) Patel, D. A.; Weller, A. M.; Chevalier, R. B.; Karos, C. A.; Landis, E. C. Ordering and defects in self-assembled monolayers on nanoporous gold. *Appl. Surf. Sci.* **2016**, *387*, 503−512.
(65) Morshed, M. N.; Asadi Miankafshe, M.; Persson, N.-K.; Behary, N.; Nierstrasz, V. A. Development of a multifunctional graphene/Fe-loaded polyester textile: robust electrical and catalytic properties. *Dalton Transactions* **2020**, *49* (47), 17281−17300.
(66) Teli, M.; Kale, R. D.; Bhatt, L. Effect of nanoclay loading on zeta potential of polyester nanocomposite fibre. *Indian Journal of Fibre & Textile Research (IJFTR)* **2017**, *42* (2), 125−131.
(67) Adamczyk, Z.; Michna, A.; Szaraniec, M.; Bratek, A.; Barbasz, J. Characterization of poly(ethylene imine) layers on mica by the streaming potential and particle deposition methods. *J. Colloid Interface Sci.* **2007**, *313* (1), 86−96.
(68) Mészáros, R.; Thompson, L.; Bos, M.; De Groot, P. Adsorption and electrokinetic properties of polyethylenimine on silica surfaces. *Langmuir* **2002**, *18* (16), 6164−6169.
(69) Marmisollé, W. A.; Capdevila, D. A.; de la Llave, E.; Williams, F. J.; Murgida, D. H. Self-Assembled Monolayers of NH2-Terminated Thiolates: Order, pKa, and Specific Adsorption. *Langmuir* **2013**, *29* (17), 5351−5359.
(70) Wang, J.-Y.; Chen, L.-C.; Ho, K.-C. Synthesis of Redox Polymer Nanobeads and Nanocomposites for Glucose Biosensors. *ACS Appl. Mater. Interfaces* **2013**, *5* (16), 7852−7861.
(71) Merchant, S. A.; Meredith, M. T.; Tran, T. O.; Brunski, D. B.; Johnson, M. B.; Glatzhofer, D. T.; Schmidtke, D. W. Effect of mediator spacing on electrochemical and enzymatic response of ferrocene redox polymers. *J. Phys. Chem. C* **2010**, *114* (26), 11627−11634.
(72) Paul, A.; Borrelli, R.; Bouyanfif, H.; Gottis, S.; Sauvage, F. Tunable Redox Potential, Optical Properties, and Enhanced Stability of Modified Ferrocene-Based Complexes. *ACS Omega* **2019**, *4* (12), 14780−14789.

https://doi.org/10.1021/acs.langmuir.1c01070
Langmuir 2021, 37, 10902−10913